The 9th European Congress on Computational Methods in Applied Sciences and Engineering
ECCOMAS Congress 2024
3 – 7 June 2024, Lisboa, Portugal

COUPLING CFD WITH 1D MODEL FOR THE PREDICTION OF PERFORMANCE OF A HEMODIALYSIS MODULE WITH UNDULATED FIBERS

ANGELO GIORDANO[*], NUNZIO CANCILLA[*], MICHELE CIOFALO[*], DANILO DONATO[†], GASPARE MAROTTA[†], ALESSANDRO TAMBURINI[*] AND GIORGIO MICALE[*]

[*] Dipartimento di Ingegneria
Università degli Studi di Palermo
Viale delle Scienze Ed. 6, 90128 Palermo, Italy

[†] Mozarc Medical®
via Camurana 1, 41037 Mirandola, Modena, Italy

Key words: Hemodialysis, Computational Fluid Dynamics (CFD), fiber undulation, fluid mechanics, Sherwood number, mass transfer efficiency.

Summary. A novel multi-scale model to determine the effect of fiber undulation on the mass transfer efficiency of a hemodialysis module has been developed and validated against experimental data.

1 INTRODUCTION

Hemodialysis is a medical treatment applied to patients with End-Stage Renal Disease (ESRD). Its impact on global healthcare is noticeable: in a work published in 2015, indeed, it has been estimated that, worldwide, in 2010, more than 2.5 million people received renal replacement therapies while approximately 6 million people could not receive the renal replacement therapies that they needed [1] and, in 2017, chronic kidney diseases accounted for around 1.2 million deaths globally [2].

Hemodialysis consists in circulating the patient's blood, rich in toxins, inside a device called hemodialyzer (or hemodialysis module), a hollow fiber membrane module which allows for blood purification. The module consists in a cylindrical polymeric housing containing ~10,000 hollow fibers. Blood flows inside the fibers in the *lumen* (or blood) side. A rinsing fluid, called dialysate, flows in the *shell* (or dialysate) side, i.e. outside the fibers and inside the polymeric housing, in counter-current mode. Dialysate is a solution of ultrapure water containing dissolved electrolytes and other substances in concentrations that ensure isotonicity with blood. Typical values of flow rates are 300 ml/min and 500 ml/min, for blood and dialysate respectively. Thanks to the separation ensured by membranes, the transport of solutes from the patient's blood to the dialysate is realized, while ensuring no direct contact between the two fluids. According to the fact that the solute transport mechanisms involve pure diffusion, pure convection, or a combination of them, the treatment is called hemodialysis, hemofiltration or hemodiafiltration, respectively. Hollow fibers used in a hemodialyzer are typically asymmetric porous membranes with outer diameter ranging from 260 to 280 μm. In commercial modules

used for adults, the diameter of the cylindrical housing is of 3-4 cm. A typical commercial module, with indication of inlet and outlet ports, along with the fluid flow directions, is sketched in **Figure 1**.

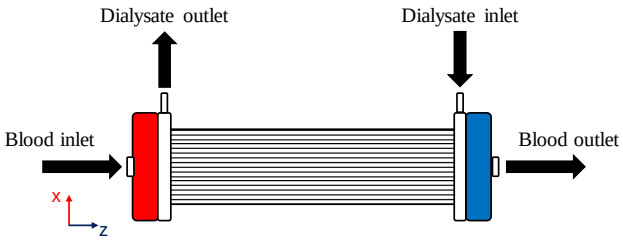

Figure 1: Sketch of a hemodialysis module. Blood and dialysate flow directions along with inlet and outlet ports are indicated. Reference axes used in the module-scale model are also shown.

The membrane module is the core of the mass transfer process. Improving mass transfer conditions is of considerable importance to enhance the performance of the treatment. In the early 2000s, several papers reported experimental works demonstrating that the use of undulated fibers is a possible way to improve the module mass transfer efficiency. In 2000, Ronco *et al.* [3] reported increased values of clearance (a performance parameter representative of the treatment efficiency in the solute removal) when utilizing modules with wavy fibers, in the so-called Moiré structure. The authors showed that wavy fibers improved the shell-side flow field distribution, thus reducing channeling phenomena. In 2003, also Leypoldt *et al.* [4] demonstrated that wavy-shaped fibers improved the solute clearance of ~10%, both for urea and creatinine. Also, the mass transfer-area coefficient K_0A, representing the reciprocal of the diffusive mass transport resistance of a solute through the membrane, increased by ~40%.

Many works on the modeling of fluid dynamics and mass transfer in fiber bundles are currently available in the literature. Among others, Dierickx et al. [5] developed a model able to predict flow and mass transfer in fiber bundles arranged both in hexagonal and square lattices in cross-flow conditions [5]. Bao and Lipscomb modeled mass transfer around bundle of fibers arranged in random distributions, assuming both an imposed wall concentration [6] and an imposed wall flux [7]. Cancilla et al. modeled both uniform [8] and non-uniform [9] bundles of fibers, in different flow conditions [10], focusing on the effects of channeling on hydrodynamics and mass transfer.

Recently, Sangeetha *et al.* [11] carried out single fiber simulations of undulated fibers with different wavelengths and amplitudes using a finite element method. The authors reported a higher clearance value for undulated fibers with respect to straight fibers. They performed simulations with: (i) undulated fibers having fixed length of 56 mm, fixed amplitude of 0.2 mm and number of crimp count (i.e. number of half-cycles of the wave) varying between 1, 2, 4 and 8 and (ii) undulated fibers having fixed length of 56 mm, fixed crimp count of 8 and amplitude varying between 0.2, 0.4, 0.6 and 0.8 mm. Results showed better performances with the shortest wavelength and the highest amplitude simulated. However, the fibers were not considered to be part of a bundle.

To the best of the authors' knowledge a fully predictive whole module model including the effects of fiber undulation derived at small-scale (single fiber) level on mass transfer performance, considering also the presence of nearby fibers of the bundle, is still lacking. The

aim of the present work was to fulfill this gap in the literature, developing a multi-scale model of a hemodialyzer with undulated fibers. The model was validated against experimental data measured on commercial fibers.

2 METHODOLOGY

The present work employs a multi-scale approach. The resulting model includes a 3-D Computational Fluid Dynamics (CFD) model, hereafter referred to as fiber-scale model, which determines the effect of fiber undulation at fiber scale and is implemented in ANSYS CFX® 2024 R1 [12], and a 1-D model, hereafter referred to as module-scale model, which translates the effect of fiber undulation at module scale and is implemented in Python. The fiber-scale model takes as input the flow conditions, the physical and the geometrical properties of the undulated fiber bundle and outputs the mass transfer efficiency (Sherwood number) associated with the investigated case. The Sherwood number is then given as input to the module-scale model, along with other operating parameters related to hemodialysis treatment, and outputs the concentration and pressure profiles along the module and the resulting clearance (the most widely used module performance indicator in hemodialysis). The quantities mentioned will be defined in the following section. A flow chart of the multi-scale model is shown in **Figure 2**.

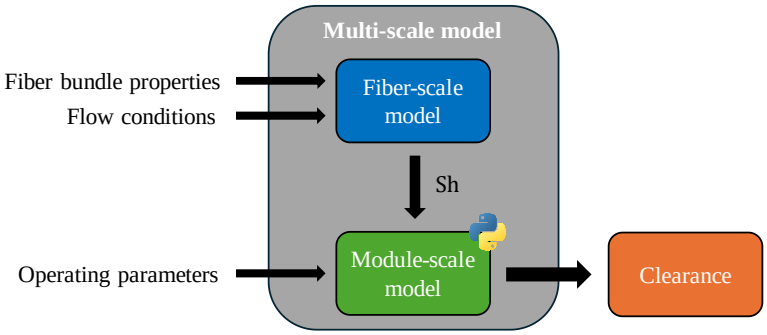

Figure 2: Flow chart of the multi-scale model. Inputs and outputs to and from both models are shown.

2.1 Main definitions

In this work, the clearance for the generic solute i, CL_i, is defined as:

$$CL_i = \frac{Q_{B,in}c_{Bi,in} - Q_{B,out}c_{Bi,out}}{c_{Bi,in}} \quad (1)$$

in which $Q_{B,in}$ and $Q_{B,out}$ are the blood flow rates at the inlet and the outlet of the module, respectively; $c_{Bi,in}$ and $c_{Bi,out}$ are the blood concentrations of the generic solute i at the inlet and the outlet of the module, respectively.

The shell-side Reynolds number, $\mathrm{Re}_{D,\sigma}$, is defined as:

$$\mathrm{Re}_{D,\sigma} = \frac{\rho_D v_\sigma \varepsilon_D d_h}{\mu_D} \quad (2)$$

where ρ_D and μ_D are the density and dynamic viscosity of the shell-side fluid, respectively, v_σ is the velocity along direction σ and d_h is the hydraulic diameter, here defined as,

$$d_h = \frac{4V_D}{S_D} \tag{3}$$

in which V_D is the shell-side fluid volume and S_D is the wet surface of the computational shell-side domain. Finally, ε_D is the shell-side porosity, defined as:

$$\varepsilon_D = \frac{V_D}{V_{tot}} \tag{4}$$

where V_{tot} is the total volume occupied by the fiber bundle (fibers + fluid).

In this work, the shell-side Sherwood number, $\mathrm{Sh}_{D,i}$, relative to the generic solute i is defined as:

$$\mathrm{Sh}_{D,i} = \frac{k_{D,i} d_h}{D_{D,i}} \tag{5}$$

where $k_{D,i}$ and $D_{D,i}$ are the average shell-side mass transfer coefficient and the diffusivity of the generic solute i in the dialysate, respectively. In its turn, the average shell-side mass transfer coefficient $k_{D,i}$ is calculated as

$$k_{D,i} = \frac{\bar{J}}{\bar{c}_{D,i,wall} - c_{D,i,bulk}} \tag{6}$$

where $\bar{J}$ is the imposed wall-averaged molar flux at the membrane wall, and $\bar{c}_{wall}$ and c_{bulk} are the wall-averaged solute concentration at the wall and the bulk concentration, respectively.

For the *lumen*-side, the Sherwood number and Reynolds number are computed using the same equations (2) and (5), substituting the relevant fluid properties of dialysate with those of blood (see Table 1), imposing a porosity equal to 1 and using the internal fiber diameter d_{int} instead of the hydraulic diameter d_h. In this case, in all quantities, the pedex *D* is substituted by *B*.

2.2 Fiber-scale model

The fiber-scale model implements the continuity, momentum and scalar transport equation in both the *lumen*-side and the shell-side. For the *lumen*-side, the computational domain is the fluid inside a single undulated fiber. For the shell-side, the computational domain is the fluid surrounding a single undulated fiber of the bundle (unit cell). The whole bundle is assumed to be constituted by the periodic repetition of this unit cell in all directions, arranged in a regular hexagonal lattice. **Figure 3.a** shows a 2-D schematic representation of a portion of a bundle, including both the blood- and the shell-side fluids. **Figure 3.b** shows a 3-D representation of the shell-side unit cell (computational domain).

The *lumen*- and shell-side fiber-scale models were based on the following simplifying assumptions:

1. All fibers are identical in dimensions and properties;
2. Fluids are modeled as incompressible and Newtonian;
3. The flow is laminar, steady and fully developed;
4. The physical properties of the fluids are constant everywhere (their changes, associated with the small changes in concentration involved in the present simulations, are considered to be negligible).

For the shell-side model, an additional simplifying assumption was made:

5. The fibers are arranged in a regular hexagonal lattice with uniform porosity.

The validity of assumptions 1-3 allows to use the Unit Cell (UC) approach to study the domain of interest. Specifically, the assumption of fully developed flow allows to split some of the variables (pressure, concentration) into a spatially periodic component, repeating identically in each UC, and a large scale component allowing for a streamwise variation of such variables. For a more detailed description of the method, the reader is referred to [8].

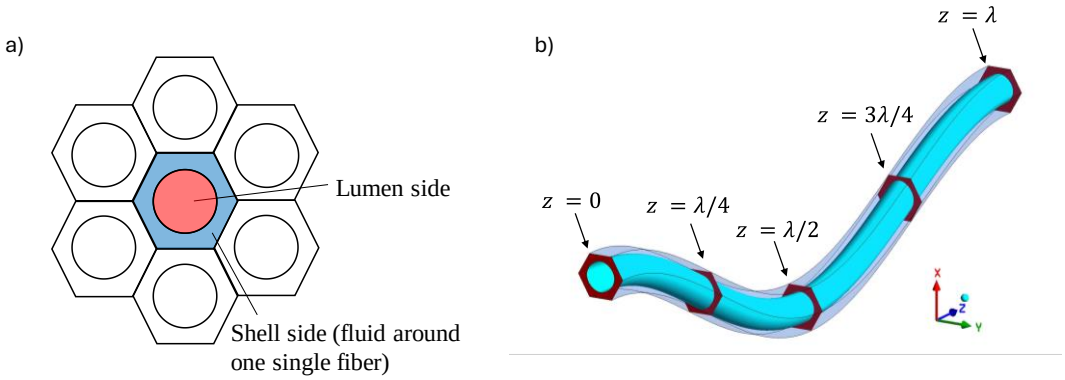

Figure 3: a) Cross sectional view of a portion of a fibers bundle arranged in a regular hexagonal lattice. Blue: shell-side fluid; red: *lumen*-side fluid. The fluid regions and the relative fibers adjacent to the simulated unit cell are also shown. b) 3-D view of a generic shell-side computational domain (amplitude $A = 0.56$ mm and wavelength $\lambda = 6.72$ mm). Some cross-sectional planes for given fractions of the wavelength are also indicated.

Based on these assumptions, the resulting continuity, momentum and scalar transport equations can be written for both models as:

$$\nabla \cdot \vec{u} = 0 \tag{7}$$

$$\rho\vec{u} \cdot \nabla\vec{u} = -\nabla\tilde{p} + \mu\nabla^2\vec{u} + \vec{F} \tag{8}$$

$$\vec{u} \cdot \nabla\tilde{c} = D\nabla^2\tilde{c} + S_c \tag{9}$$

where $\vec{u}$ is the velocity vector, $\tilde{p}$ is the periodic component of pressure, $\vec{F}$ is a forcing term (driving pressure gradient) compensating the large scale pressure loss, $\tilde{c}$ is the periodic component of the concentration and S_c is a source term compensating the large scale concentration gradient.

Since the unit cell approach was used, periodic boundary conditions were imposed to all variables between opposite surfaces of the computational fluid domain. A no slip condition was imposed to the surface of the fiber wall, along with a Neumann boundary condition to the concentration field, which corresponds to a constant wall mass flux that was arbitrarily set to $\pm 10^{-4}$ mol·m^{-2}·s^{-1} (minus sign for the blood and plus for the dialysate). The value of the pressure gradient in the z direction was dynamically adjusted as to obtain a given longitudinal Reynolds number (1 and 10 for the *lumen*- and blood-side, respectively). The boundary conditions are summarized in **Figure 4**. Preliminary simulations showed that a single precision solver yielded results with a discrepancy of less than ±1% compared to a double precision one; therefore, a single precision solver was used for the final runs.

A grid-independence analysis revealed that grids with ~4 million volumes (with ~40,000 finite volumes in the cross section and 100 volumes along the fiber longitudinal axis) guarantee a discrepancy in the results lower than 1% with respect to the finest grid tested.

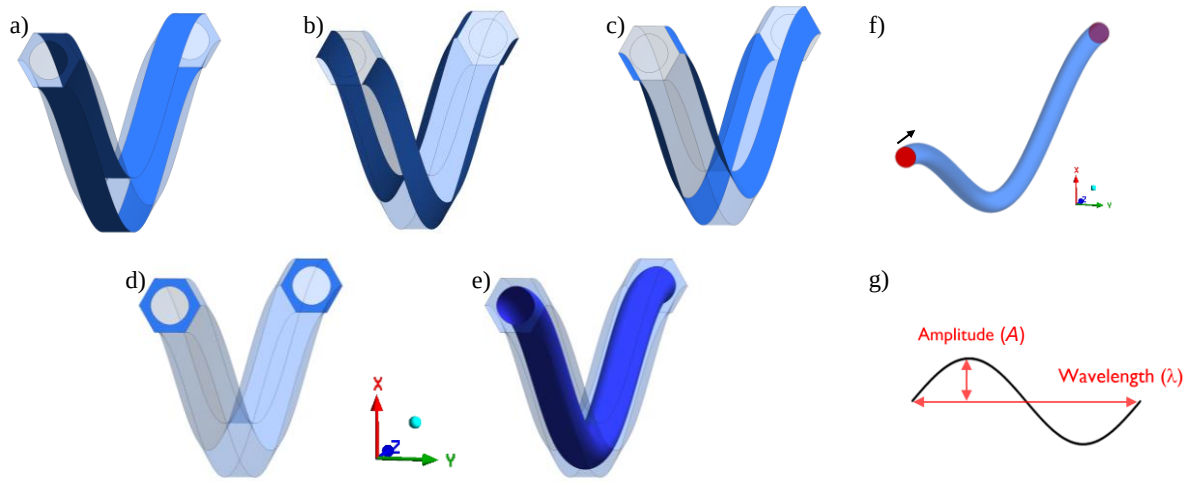

Figure 4: Boundary conditions for the (a-e) shell- and (f) *lumen*-side geometries. (a-e) Surfaces of the computational domain along the (a) *x* direction, (b-c) *y* directions and (d) *z* direction, to which the translational periodicity was applied (in each figure the two periodic boundaries are depicted in blue). e) Cylindrical surface of the fiber wall to which the conditions of no slip and constant mass flux were applied. (f) The red surfaces are planes to which the periodic boundary condition was applied. The fiber wall (blue) is the surface to which the conditions of no slip and constant mass flux were applied. The black arrow indicates the *z* direction along which the pressure gradient was imposed. (g) Indication of the amplitude *A* and wavelength λ: (a-e) λ=6.72 mm and *A*=0.56 mm; (f) λ=7.224 mm and *A*=0.392 mm.

2.3 Module-scale model

As anticipated at the beginning of Section 2, the model uses the Sherwood number calculated by the fiber-scale model as input to compute the shell-side mass transfer coefficient k_D. This data is then used to solve the mass balance equations, coupled with the convective-diffusive mass transport equations.

The module-scale model was based on the following assumptions:

1. The transport across the radial and azimuthal directions of the module is neglected, and only axial transport along the *z* direction (see **Figure 1**) is considered;
2. All fibers are identical and regularly distributed across the volume of the module, hence the behavior of the whole module can be extrapolated from the behavior of a single fiber and its surrounding fluid;
3. The physical properties of the fluids are constant along the module length (effects due to changes in concentration are neglected);
4. Changes in the flow rates are attributed only to the water flowing by ultrafiltration from one compartment to the other of the module;
5. The undulated fibers are straightened for the calculation of the fibers surface area;
6. The system is at steady state;
7. The flow regime in both the *lumen*- and the shell-side is laminar and the fluids are

Newtonian;

8. The formation of concentration polarization layers is neglected;
9. The shell-side fluid is considered to flow through a porous medium.

Based on these assumptions, the overall mass balance equations were written as:

$$\frac{dQ_B}{dz} = -J_{uf}(z)\pi d_{ext}N \tag{10}$$

$$\frac{dQ_D}{dz} = -J_{uf}(z)\pi d_{ext}N \tag{11}$$

in which Q_B and Q_D are the blood- and dialysate-side flow rates, respectively, d_{ext} is the external fiber diameter, N is the number of fibers in the bundle. J_{uf} is the ultrafiltration flux, defined as:

$$J_{uf}(z) = L_P(p_B(z) - p_D(z) - p_{onc}) \tag{12}$$

where L_P is the membrane hydraulic permeability, p_B and p_D are the lumen- and shell-side pressure values at the generic position z, respectively and p_{onc} is the oncotic pressure of the proteins in the blood. This latter was set to 0 Pa in all simulations performed in this work.

The component mass balance equations, relative to the solute i, are:

$$Q_B\frac{dc_{B,i}}{dz} = -J_{d,i}(z)N\pi d_{int} - J_{uf}N\pi d_{ext}c_{m,i}(z)(1-\sigma_i) \tag{13}$$

$$Q_D\frac{dc_{D,i}}{dz} = -J_{d,i}(z)N\pi d_{int} - J_{uf}N\pi d_{ext}c_{m,i}(z)(1-\sigma_i) \tag{14}$$

in which $c_{B,i}$ and $c_{D,i}$ are the blood- and dialysate-side concentrations of the solute i, respectively, $c_{m,i}$ is the solute i concentration in the fluid crossing the membrane, imposed equal to $c_{B,i}$ when $J_{uf} > 0$ and to $C_{D,i}$ when $J_{uf} < 0$, σ_i is the Staverman's reflection coefficient of the solute i, and $J_{d,i}$ is the molar diffusive mass flux. This latter is defined as:

$$J_{d,i}(z) = U_i(c_B(z) - c_D(z)) \tag{15}$$

where U_i is the overall mass transfer coefficient for the solute i, which is expressed as:

$$\frac{1}{U_i} = \frac{1}{k_{D,i}} + \frac{1}{k_{m,i}} + \frac{1}{k_{B,i}} \tag{16}$$

in which $k_{D,i}$ and $k_{B,i}$ are the dialysate- and blood-side mass transfer coefficient computed by the fiber-scale CFD model, while $k_{m,i}$ is the diffusive mass transfer coefficient for the solute i in the membrane. The value of this quantity has been obtained by fitting experimentally measured data provided by Mozarc Medical® and using the present model with preliminary simulations. Specifically, the Levenberg-Marquardt non-linear least square regression algorithm was used.

The pressure profiles are computed by means of the Hagen-Poiseuille (*lumen*-side) and the Darcy (shell-side) equations, solving the following differential equations:

$$\frac{dp_B}{dz} = \frac{128\mu_B Q_B(z)}{\pi d_{int}^4} \tag{17}$$

$$\frac{dp_D}{dz} = \frac{\mu_D Q_D(z)}{K_{Darcy}\frac{\pi D_{shell}^2}{4}} \tag{18}$$

where p_B and p_D are the blood- and dialysate-side pressures, respectively, K_{Darcy} is the shell-side superficial Darcy permeability (i.e. referred to the whole surface of the computational domain, including fibers and fluid) and D_{shell} is the diameter of the module shell.

The Darcy permeability K_{Darcy} has been previously experimentally determined with pressure drop measurements on commercial modules at different bundle porosities. The full results are not reported here for brevity. The derived empirical correlation obtained from the fitting of the experimental data of the Darcy permeability K_{Darcy} as a function of porosity ε_D, expressed in m^2, is:

$$K_{Darcy} = 2 \cdot 10^{-11} e^{8.97\varepsilon_D} \tag{19}$$

Finally, the total ultrafiltration flow rate has been computed as:

$$Q_{uf} = \int_0^L J_{uf}(z)\pi N d_{ext} dz \tag{20}$$

in which L is the length of the fiber bundle.

This set of equations was solved with Euler's method in Python. A discretization of the module in the z direction into 1000 intervals has shown to guarantee grid-independent results (discrepancy lower than 1% with respect to the finest discretization employed). The value of N was chosen as to give the desired value of porosity in each simulation.

3 RESULTS

Urea was chosen as reference solute in all runs. Membrane and physical fluids properties used are listed in **Table 1**.

Table 1: Membrane and physical fluids properties used in the present work. Fluid properties refer to urea (solute used in the present work).

ρ_D, ρ_B [kg/m^3]	1000	D_D [m^2/s]	$1.81 \cdot 10^{-9}$ [13]
μ_D [Pa·s]	$8.9 \cdot 10^{-4}$ [14]	D_B [m^2/s]	$7.4 \cdot 10^{-10}$ [15]
μ_B [Pa·s]	$3.5 \cdot 10^{-3}$ [15]	σ [-]	0
k_B [m/s]	$3.95 \cdot 10^{-5}$*	L_P [ml/m^2/h/mmHg]	260
k_D [m/s]	$8.36 \cdot 10^{-5}$*	d_{int} [m]	$2.0 \cdot 10^{-4}$
k_m [m/s]	$8.22 \cdot 10^{-6}$**	d_{ext} [m]	$2.8 \cdot 10^{-4}$

*Derived from the fiber-scale model results

**Obtained by the fitting of experimental data provided by Mozarc Medical® relative to commercial modules

In the *lumen*-side, simulations for fiber geometries with different amplitude and wavelength showed that, at Reynolds number equal to 1 (a typical value in hemodialysis), the *lumen*-side Sherwood number was constant and equal to 4.36. This value corresponds to the Sherwood number value derived by the analytic solution for fully developed laminar flow regimes in a straight pipe, with imposed wall flux boundary condition[16]. For this reason, $Sh_{B,urea}$ = 4.36 was used in all cases.

3.1 Model validation

The multi-scale model was validated against experimental clearance data provided by Mozarc Medical®. The data referred to a hemodialysis module with $\lambda/d_{ext} = 28.9$, $A/d_{ext} = 0.72$, $N = 11150$ (resulting in $\varepsilon_D = 0.378$), $L = 0.241$ m. The dialysate flow rate is $Q_D = 500$ ml/min, $Q_{uf} = 10$ ml/min and the membrane and fluids properties are as in **Table 1**. For this fiber geometry, the Sherwood number predicted by the fiber-scale model was $Sh_D = 8.3$.

Model predictions along with experimental data are reported as a function of the inlet blood flow rate in **Figure 5**. The model predictions well agree with the experimental clearance values (reported together with the dispersion bars). As expected, clearance increases as the inlet blood flow rate increases. Clearance profiles tend to flatten at highest blood flow rates.

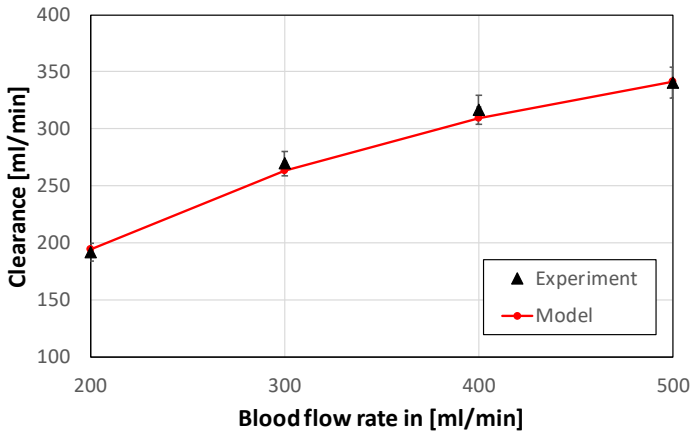

Figure 5: Urea clearance predicted by the multi-scale model (line with circles) compared with experimental data (triangles) as a function of the inlet blood flow rate. In the experiments, dispersion bars are indicated.

3.2 Fiber-scale model results

Results reported here refer to the simulations of the shell-side fluid at porosity $\varepsilon_D = 0.5$ and $\mathrm{Re} = 10$. Fibers with $A/d_{ext} = 2$ and $\lambda/d_{ext} = 24$ are considered. **Figure 6** shows maps of velocity w with vector plots and urea concentration for given cross-sectional plane positioned at $z = 0$ and $z = \lambda/4$ (see **Figure 3b** for planes location). Orthogonal velocities are also shown when their magnitude is not negligible. When cross sections are positioned in regions with the highest curvature (i.e., $z = \lambda/4$), both the velocity w and the concentration maps deviate with respect to the respective maps at the straight region of the fiber (i.e., $z = 0$). Specifically, areas of lower velocity and higher concentration are formed in the bottom and top parts of the hexagonal cross sections, visible in **Fig. 6b** and **Fig. 6d**, respectively, corresponding to regions in which the fluid domain between two adjacent fibers is tight. On the contrary, regions of lower concentration and higher velocity appear on the left and on the right side of the hexagonal cross section. These results suggest that mass transfer characteristics of the undulated geometry differ from those relative to straight fibers: for this geometry, the predicted shell-side Sherwood number was ~10. This value is ~3% larger than that predicted for straight fibers at the same porosity (~9.7).

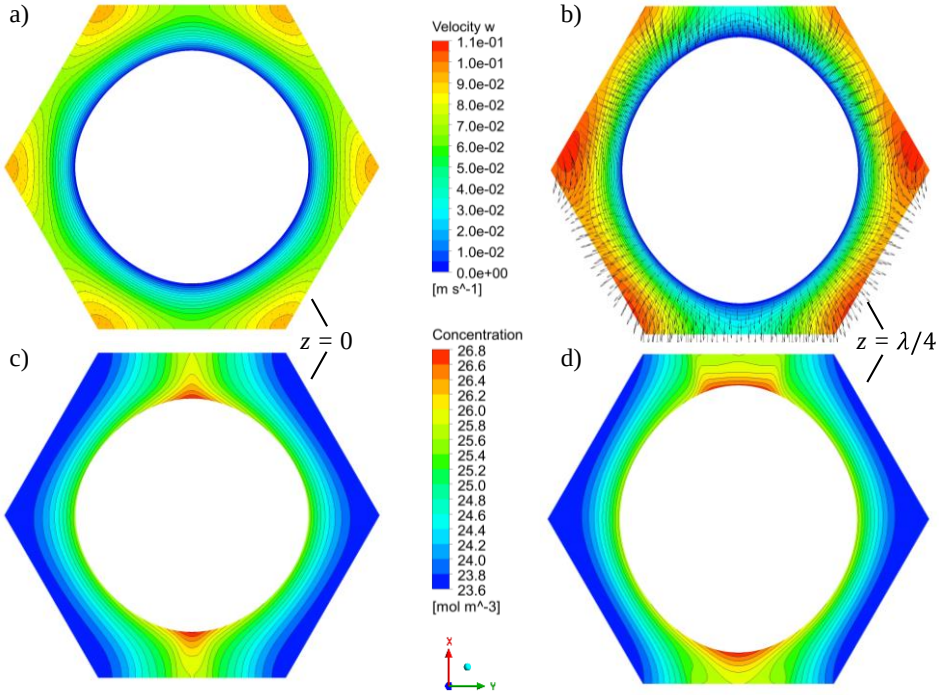

Figure 6: Maps of shell-side velocity *w* with superimposed vector plots (a, b) and of urea concentration (c, d) at different *xy* cross-sectional planes. Cross-sectional plane location: (a, c) *z* = 0; (b, d) *z* = *λ*/4.

3.3 Module-scale model results

Results reported here refer to a bundle of undulated fibers having $\lambda/d_{ext} = 24$ and $A/d_{ext} = 2$. The simulated module has $N = 8970$ fibers (which gives a porosity $\varepsilon_D = 0.5$), $D_{shell} = 0.0375$ m and $L = 0.241$ m. Imposed flow rates are $Q_B(z = 0) = 300$ ml/min, $Q_D(z = L) = 500$ ml/min and $Q_{uf} = 10$ ml/min.

Figure 7 reports concentration (map a) and pressure (map b) profiles along the dimensionless module length, defined as $l = z/L$. Blood and dialysate are fed in counter-current mode (blood enters at l = 0, dialysate at l = 1). Urea concentration in the blood was arbitrarily set to 20 mol/m^3 at the *lumen*-side inlet and to 0 in the dialysate at the shell-side inlet. **Fig. 7a** shows that, as expected, urea concentration in the blood decreases along the dimensionless module length, while the opposite is true in the dialysate. Pressure profiles shown in **Fig. 7b** permit to deduce information on the ultrafiltration flux direction. Notably, in the first half of the module length (from $l = 0$ to ~0.5), the blood pressure is higher than the dialysate one and an ultrafiltration flux goes from *lumen*- to shell-side compartment. On the other hand, in the second half of the module length (from $l =$ ~0.5 to 1), pressure in the dialysate is higher with respect to that in the blood and backfiltration occurs: the ultrafiltration flux changes direction with respect to the first half of the module length and goes from shell- to *lumen*-side compartment.

The computed urea clearance value for the undulated fibers case is 244.3 ml/min, being this latter ~0.08% larger with respect to that predicted at the same operating conditions for a module with straight fibers, corresponding to 244.1 ml/min.

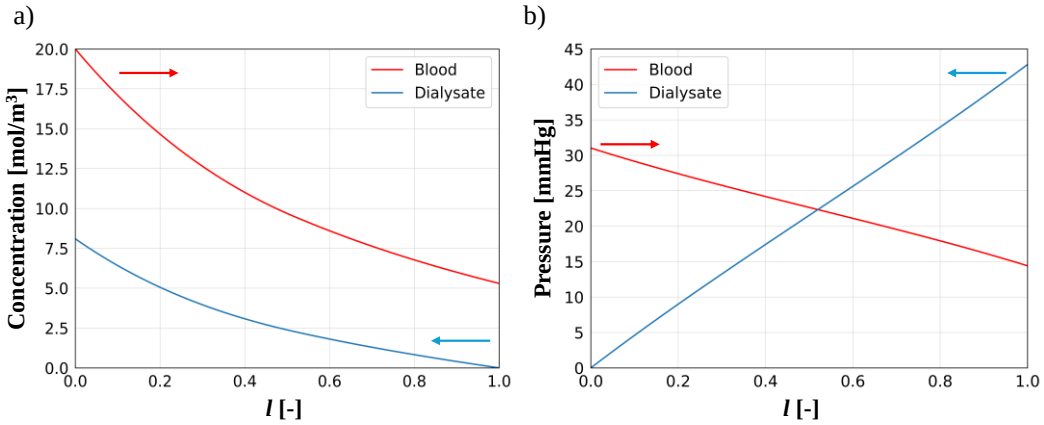

Figure 7: Urea concentration (a) and pressure (b) profiles as a function of the dimensionless module length *l*. Red and blue arrows indicated blood and dialysate flow directions, respectively.

4 CONCLUSIONS

A new multi-scale model capable of predicting the effects of fiber undulation on the mass transfer efficiency in commercial hemodialysis modules was developed and validated. A grid independence analysis revealed that grids with 4 million finite volumes and discretization of 1000 intervals in the *z* direction for the fiber- and module-scale model, respectively, were enough to guarantee grid independent results.

Simulations with the undulated fiber geometry investigated here showed an increase in shell-side Sherwood number, while *lumen*-side Sherwood number remained unaffected in all the investigated conditions. However, it is interesting to note that, despite the shell-side Sherwood number for the undulated fiber bundle is ~3% higher with respect to that obtained for the straight fibers bundle with the same porosity, the urea clearance exhibited a corresponding increase of ~0.08% only. This can be explained by acknowledging that the shell-side mass transfer resistance (see Eq. 16) is not the controlling one in the hemodialysis process. However, technologies with similar geometries but different mass transfer conditions may take greater benefits from the results presented. Nonetheless, it is also important to note that even small improvements in clearance can be significant for the market of hemodialysis modules. Furthermore, the present model can be used to explore a wide range of geometries and operating conditions (different amplitudes, wavelengths, porosities, flow rates, etc.) which may bring to a clearance increase of higher significance. In fact, preliminary results showed that a proper combination of such parameters could improve the shell-side mass transfer efficiencies to a larger extent. This will be the subject of a future work.

REFERENCES

[1] T. Liyanage, T. Ninomiya, V. Jha, B. Neal, H. M. Patrice, I. Okpechi, M. Zhao, J. Lv, A. X. Garg, J. Knight, *et al.*, "Worldwide access to treatment for end-stage kidney disease: a systematic review," *Lancet Lond. Engl.*, vol. 385, no. 9981, pp. 1975–1982, May 2015, doi: 10.1016/S0140-6736(14)61601-9.

[2] B. Bikbov, C. A. Purcell, A. S. Levey, M. Smith, A. Abdoli, M. Abebe, O. M. Adebayo, M. Afarideh, S. K. Agarwal, M. Agudelo-Botero, *et al.*, "Global, regional, and national

burden of chronic kidney disease, 1990–2017: a systematic analysis for the Global Burden of Disease Study 2017," *The Lancet*, vol. 395, no. 10225, pp. 709–733, Feb. 2020, doi: 10.1016/S0140-6736(20)30045-3.

[3] C. Ronco, A. Brendolan, C. Crepaldi, M. Rodighiero, P. Everard, M. Ballestri, G. Cappelli, M. Spittle, and G. La Greca, "Dialysate Flow Distribution in Hollow Fiber Hemodialyzers with Different Dialysate Pathway Configurations," *Int. J. Artif. Organs*, vol. 23, no. 9, pp. 601–609, Sep. 2000, doi: 10.1177/039139880002300902.

[4] J. K. Leypoldt, A. K. Cheung, T. Chirananthavat, J. F. Gilson, C. D. Kamerath, and R. B. Deeter, "Hollow Fiber Shape Alters Solute Clearances in High Flux Hemodialyzers," *ASAIO J.*, vol. 49, no. 1, p. 81, Feb. 2003.

[5] P. W. Dierickx, D. S. De Wachter, and P. R. Verdonck, "Two-Dimensional Finite Element Model for Oxygen Transfer in Cross-Flow Hollow Fiber Membrane Artificial Lungs," *Int. J. Artif. Organs*, vol. 24, no. 9, pp. 628–635, Sep. 2001, doi: 10.1177/039139880102400904.

[6] L. Bao and G. G. Lipscomb, "Mass transfer in axial flows through randomly packed fiber bundles with constant wall concentration," *J. Membr. Sci.*, vol. 204, no. 1, pp. 207–220, Jul. 2002, doi: 10.1016/S0376-7388(02)00043-1.

[7] L. Bao and G. G. Lipscomb, "Well-developed mass transfer in axial flows through randomly packed fiber bundles with constant wall flux," *Chem. Eng. Sci.*, vol. 57, no. 1, pp. 125–132, Jan. 2002, doi: 10.1016/S0009-2509(01)00368-2.

[8] N. Cancilla, L. Gurreri, G. Marotta, M. Ciofalo, A. Cipollina, A. Tamburini, and G. Micale, "CFD prediction of shell-side flow and mass transfer in regular fiber arrays," *Int. J. Heat Mass Transf.*, vol. 168, p. 120855, Apr. 2021, doi: 10.1016/j.ijheatmasstransfer.2020.120855.

[9] N. Cancilla, L. Gurreri, M. Ciofalo, A. Cipollina, A. Tamburini, and G. Micale, "Hydrodynamics and mass transfer in straight fiber bundles with non-uniform porosity," *Chem. Eng. Sci.*, vol. 279, p. 118935, Sep. 2023, doi: 10.1016/j.ces.2023.118935.

[10] N. Cancilla, M. Ciofalo, A. Cipollina, A. Tamburini, and G. Micale, "Straight fiber bundles with non-uniform porosity: Shell-side hydrodynamics and mass transfer in cross flow," *Chem. Eng. Sci.*, vol. 291, p. 119947, Jun. 2024, doi: 10.1016/j.ces.2024.119947.

[11] M. S. Sangeetha, A. Kandaswamy, C. Lakshmi Deepika, and C. V. Revanth, "Finite Element Analysis For Comparing The Performance Of Straight And Undulated Fibers In Altering The Filtering Efficiency Of Hemodialyzer Membranes," *J. Mech. Med. Biol.*, vol. 19, no. 05, p. 1850063, Aug. 2019, doi: 10.1142/S021951941850063X.

[12] "ANSYS, 2024. ANSYS CFX Reference Guide 2024 R1."

[13] E. Klein, F. Holland, A. Lebeouf, A. Donnaud, and J. K. Smith, "Transport and mechanical properties of hemodialysis hollow fibers," *J. Membr. Sci.*, vol. 1, pp. 371–396, Jan. 1976, doi: 10.1016/S0376-7388(00)82283-8.

[14] R. H. Perry and D. W. Green, Eds., *Perry's chemical engineers' handbook*, 8. ed. New York, NY: McGraw-Hill, 2008.

[15] S. Middleman, *Transport phenomena in the cardiovascular system*. in Wiley Interscience series on biomedical engineering. New York: Wiley-Interscience, 1972.

[16] F. P. Incropera and D. P. DeWitt, *Fundamentals of heat and mass transfer*, 4. ed. New York, NY [u.a]: Wiley, 1996.